Reconciling disparate 20th Century Indo-Pacific ocean temperature trends in the instrumental record

Amy Solomon and Matthew Newman

PSD/ESRL/NOAA and CDC/CIRES/University of Colorado

email:amy.solomon@noaa.gov

submitted January 17, 2012, revised May 9, 2012,

Nature Climate Change

Abstract

Large discrepancies exist between 20th century tropical Indo-Pacific sea surface temperature (SST) trends determined from current reconstructions. These discrepancies prevent an unambiguous verification and validation of climate models used for projections of future climate change. In this study we demonstrate that a more consistent and robust trend among all the reconstructions is found by filtering each dataset to remove ENSO, which is represented not by a single index time series but rather by an evolving dynamical process. That is, the discrepancies appear largely the result of different estimates of ENSO variability in each reconstruction. The robust ENSO-residual trend pattern represents a strengthening of the equatorial Pacific temperature gradient since 1900, due to a systematic warming trend in the warm pool and weak cooling in the cold tongue. Similarly, the ENSO-residual sea level pressure trend represents no weakening of the equatorial Walker circulation over the same period. Additionally, none of the disparate estimates of post-1900 total eastern equatorial Pacific SST trends are larger than can be generated by statistically stationary, stochastically forced empirical models that reproduce ENSO evolution in each reconstruction.

Given the impact of sea surface temperature (SST) anomalies in the tropical Indo-Pacific on climate worldwide[1,2,3], identifying systematic and predictable externally-forced trends in this region is essential to future regional climate change projections. Accurately characterizing natural vs. forced SST variability in observations is also needed to validate climate model hindcasts of the 20th Century and then to assess climate model projections of the 21st Century[4]. It is thus a concern that large discrepancies in estimated tropical Indo-Pacific 20th century trends exist between observationally-based SST reconstructions[5] (Fig. 1). While warming trends in the Indian Ocean and western Pacific Ocean are consistent across the 4 datasets, it is uncertain whether eastern equatorial Pacific SSTs are undergoing long-term warming or cooling, a fundamental issue within theories of the tropical response to anthropogenic climate change[6,7].

There are competing theories for the response of the tropical Pacific Ocean to an increase in greenhouse gases. Assuming a uniform heating of the tropical Pacific, enhanced upwelling of cold water that dominates over local surface radiative heating in the east equatorial Pacific will cause the western Pacific to warm faster than the eastern Pacific, enhancing the equatorial SST gradient, increasing surface wind divergence over the eastern Pacific and surface equatorial easterlies, thereby enhancing the eastern equatorial upwelling—the ocean dynamical thermostat hypothesis[8-11]. Alternatively, as the climate warms, the cooling effect of surface evaporative cooling in the west will increase while the cooling due to vertical advection in the east may decrease due to an increase in subsurface temperatures. The resulting reduction in the equatorial SST gradient drives a reduction in the surface equatorial easterlies, thereby reducing the upwelling in the eastern equatorial Pacific[12-14]. In addition, from an atmospheric perspective, an increase in specific humidity in Clausius-Clapeyron relationship with increasing SSTs may not be matched by a proportional increase in precipitation[15], requiring a slowdown of the Walker circulation and a corresponding relaxation of the equatorial SST gradient[16]. How the tropical Pacific will respond to an increase in greenhouse gases has significant implications for global climate change[17,18]

ENSO is the dominant mode of interannual tropical variability. Fig. 2 shows the canonical peak ENSO anomaly pattern, with maximum SSTs along the central and eastern equatorial Pacific and opposite sign anomalies extending from the Maritime Continent to the subtropics. The time series associated with this pattern (Fig. 2d) shows the broadband nature of ENSO variability[19], with discrete events occurring every 2-7 years. ENSO is also related to tropically-averaged SST anomalies. This is seen in domain-averaged tropical Indo-Pacific SST anomalies (Fig. 2d) that closely follow ENSO variability over the last 50 years, suggesting that estimating the tropical Indo-Pacific Ocean response to slowly evolving changes in external forcing requires removing sampling biases due to irregular large-amplitude ENSO events.

Separating ENSO variability from the response to external forcing is challenging not least due to the question of how to define ENSO[20]. Many studies use a single index constructed from a regional average of SSTs (e.g., the NINO3.4 [5°S-5°N, 120-170°W] or cold tongue [5°S-5°N, 90-180°W] indices[21,22]) as a measure of ENSO. One drawback of this

approach is that ENSO structure is dynamic, evolving throughout the event[20,23]. For example, large thermocline anomalies precede a number of ENSO events (such as in 1982 and 1997) and propagate eastward as Kelvin waves across the equatorial Pacific[24], often in association with more meridionally-oriented SST anomalies[25]. In ENSO's decay phase tropical SST anomalies first return to normal in the cold tongue while still persisting elsewhere[26]. In addition, using one index may conflate internal ENSO variability with an "ENSO-like" response to external forcing[4].

Here we take advantage of the fact that observed tropical SST variability is well described as "multivariate red noise", a stochastically-forced linear dynamical system where all evolving perturbations are stable to exponential growth but some can – and for ENSO, do – experience substantial transient growth and decay over finite time intervals[25]. Observed multivariate red noise, determined by a "Linear Inverse Model"[25] (LIM) constructed from the short time-lag statistics of the dataset itself, reproduces observed SST anomaly evolution statistics on time scales ranging from seasons to years better than virtually all "20th-century" IPCC AR4 coupled GCMs[19]. Because multivariate red noise provides a baseline for the statistics of observed tropical seasonal anomaly evolution, it also serves as a useful null hypothesis against which possible changes in SST can be tested[26] Motivated by these results, we have developed a novel "optimal perturbation filter" (hereafter referred to as "the filter") that uses a LIM to remove space- and time-varying ENSO anomalies from the ocean temperature data record. We demonstrate that uncertainty in tropical Indo-Pacific SST trends in different reconstructions can be explained by disparate estimates of ENSO variability, and that removing this variability results in consistent centennial trends.

Reconciling long-term SST trends

In this study, ENSO is represented by variability that evolves from the optimal initial condition $\phi_1$through a mature ENSO event including its decay phase (see Methods, below) over a period of 21 months. The *potential* growth of this initial condition is determined by an analysis of the LIM, but it is in fact realized by the *actual* evolution of observed ENSO events of both signs[25,26]. The structure of ϕ_1(Supplemental Fig. 1) from the LIM constructed using the SODA 5m temperatures shows SST anomalies in the central and eastern equatorial Pacific with weaker opposite sign anomalies extending from the Maritime Continent to the

subtropics, similar to analyses using different datasets and resolutions[19,23,25-28]. Regressing the remainder of the three-dimensional ocean temperature field on the time series of this structure (see Supplemental Fig. 1b,c) reveals that ϕ_1 anomalies maximize in the central and eastern equatorial Pacific thermocline. At 160°W, the equatorial thermocline anomaly is suggestive of equatorial Kelvin waves. This structure then rapidly evolves, reaching the ENSO mature phase in 6-9 months (not shown, but quite similar to Fig. 2a-c) with large equal but opposite equatorial thermocline anomalies in the eastern and western tropical Pacific, then decaying over the next several months[26].

When the filter is applied to the SODA dataset, the resulting ENSO-residual data at 5m (Fig. 3a) has a positive trend in the Indian Ocean, the warm pool and in the subtropics. In contrast, the cold tongue trend is near zero, and the equatorial thermocline has a pronounced cooling trend (Fig. 3b) with largest amplitude off the equator (Fig. 3c). The wind stress trend acts to shift the wind stress maximum westward, by strengthening the trades in the west and weakening them in the east. The unfiltered wind stress trend (not shown) is generally similar except along the equator from about 140ºE to 160ºW, where it is westerly instead of easterly. Also shown (Fig. 3d) are ENSO-residual and unfiltered 5m temperatures averaged over the warm pool and cold tongue regions (indicated by the boxes in Fig. 3a and lightly smoothed with a one-year running mean). The filter removes little variability in the warm pool leaving the low-frequency warming trend unchanged. On the other hand, in the cold tongue region the filter removes almost all notable ENSO events of both signs leaving a weak residual that has no trend (cf. Fig. 3a). Applying the filter to the SST reconstructions for the same period as the SODA data produces similar results: a warming trend in the warm pool that is relatively insensitive to the filter and trends in the cold tongue that are removed by the filter (results not shown).

We next turn to the four long-term SST datasets. Interestingly, small differences in the reconstructions seen in the cold tongue and warm pool averages (Fig. 4a and 4c) throughout the 1900-2010 record cause large differences in linear trends (Fig. 1), most notably in the east equatorial Pacific. We find these differences are consistent with the different LIMs constructed from each dataset. In particular, the optimal initial condition ϕ_1 can amplify by up to 20% more in the ERSST dataset than in the HadISST dataset, with the other two lying in between (results not shown). Also, very large ensembles

of 120-yr long integrations of (1) with different realizations of noise can be used to determine the 95% confidence level of the observed linear trends against multivariate red noise[26,29] shown by stippling in Fig. 1. Note that for none of the unfiltered datasets is the trend in the eastern equatorial Pacific significant by this measure; that is, the observed trends are consistent with being a residual of natural variability.

The filter is next applied to each of four SST datasets. Again, anomalies in the warm pool are relatively insensitive to the filter (cf. Figs. 4c and 4d) especially compared to its impact in the cold tongue (cf. Figs. 4a and 4b). With the ENSO variability removed, 1900-2010 trends are now much more similar across the four SST reconstructions, both in the Indian and Pacific Oceans (Fig. 5). In particular, all four reconstructions now show a cooling trend in the eastern equatorial Pacific of similar magnitude and horizontal extent, with notable warming elsewhere except in the southern Indian Ocean. Anomaly pattern correlation coefficients between trend patterns from different reconstructions all increase, from a range of 0.33-0.73 for the unfiltered datasets to a range of 0.62-0.86 for the ENSO-residual datasets. In addition, testing the significance (indicated by the stippling in Fig. 5) of the ENSO-residual trends against the multivariate red noise large ensembles, in this case also filtered, suggests that the eastern equatorial cooling is significant. Notably, applying a similar test to the ENSO-residual warm pool and cold tongue indices suggests that ENSO-residual trends in the warm pool (cold tongue) would not have been significant for time series shorter than 80 (95) years.

To identify whether there is a systematic change of the sea level pressure anomalies associated with the strengthening of the equatorial Pacific SST gradient seen in Fig. 5, we applied the filter to seasonal mean 1870-2008 HadSLP2 sea level pressure anomalies (SLP). Since ENSO variability in HadSLP2 may differ from that in HadISST, we construct a filter with SLP alone (red line in Fig. 6), as well as regressing the SLP dataset on the ENSO-residual HadISST principal components (blue dashed line in Fig. 6). We find that removing ENSO variability with the optimal perturbation filter reduces the magnitude of both the Indian Ocean/west Pacific and central-east Pacific anomalies in the 1975-2000 period so that the gradient (defined as the west-east SLP) at the end of the record does not exceed the peak around 1930 (Fig. 6). The difference between the unfiltered and ENSO-residual linear trend maps (see Supp. Fig. 24) shows that ENSO variability during the 1900-2008 period produces

a positive linear trend in the SLP gradient that is removed by the filter. Note that even without filtering, the smoothed SLP gradient decreases between 1994-2004. The ENSO-residual gradient time series has 2003-2005 values that are similar to values in the first 30 years of the record. These results suggest that in both the ENSO-residual and unfiltered gradient time series there has not been either a systematic weakening or strengthening of the "Walker circulation[30]", the zonal overturning atmospheric circulation in the tropical Indo-Pacific, over the 1900-2008 period.

Discussion

Based on estimates of centennial trends in the Indo-Pacific from reconstructions of tropical SSTs, it has been uncertain whether an increase in greenhouse gases has resulted in a strengthening or a weakening of equatorial Pacific temperature gradients[5,31]. There is likewise some uncertainty about whether the related atmospheric Walker circulation has weakened or not in the 20th century[5,16,31-34]. In this study, we have reconciled four different SST reconstructions to agree that the equatorial Pacific temperature gradient has strengthened since 1900 due to a warming trend in the warm pool. The weak cooling trend we find in the eastern equatorial Pacific cold tongue in the absence of ENSO is broadly consistent[20] with a number of previous observational studies that used a range of techniques and datasets[11,20,35,36]. By removing spurious trends due to different estimates of interannual ENSO variability, our approach yields a robust trend among all the reconstructions.

Additionally, for the shorter SODA dataset, the strengthened ENSO-residual equatorial temperature gradient is associated with strengthened trades in the western Pacific, including a weak easterly trend along the equator. Also, the ENSO-residual HadSLP2 SLP anomalies indicate that there has been no consistent weakening in the tropical Indo-Pacific SLP gradient over the 1900-2008 period. Both the SODA and HadSLP2 results appear to be inconsistent with the suggestion of a systematic weakening of the Walker circulation.

While uncertainty in the secular SST trend between the reconstructions appears due to uncertainty in ENSO variability, an ENSO component within the overall trend remains possible. However, any ENSO warming trend is so weak that its amplitude cannot be determined with statistical significance over the 111-yr record. In particular, in the ERSST dataset, the relatively larger ENSO warming must be assessed against its relatively stronger

ENSO variability. For all four reconstructions, our analysis has estimated that even with removal of ENSO *variability*, a weak positive trend in the ENSO *pattern* time series remains (that is, in the leading tropical Indo-Pacific SST principal component) but is overwhelmed by equatorial cooling in the second EOF.

The importance of this robust ENSO-residual pattern for long-term climate change extends beyond the Tropics. For example, this pattern is similar to the "perfect ocean for drought" pattern in the Indo-Pacific, the 1998-2002 tropical SST anomalies that were coincident with widespread mid-latitude drying, where both eastern equatorial Pacific cold SST anomalies and warm Indian Ocean and warm pool SST anomalies contributed to the drying over North America, southern Europe, and southwest Asia[37]. In addition, our trend pattern is similar to the predictable tropical SST trend component found in a large ensemble of externally forced (A1B scenario) NCAR Community Climate System Model Version 3 2010-2060 simulations[38], suggesting that global climate impacts driven by long-term changes in the Tropics are more likely to be predictable when they are related to this robust ENSO-residual trend.

Apparent secular trends that are a residual of a series of unfortunate ENSO events are an issue not only in nature but also in climate model simulations, where, even for extreme forcing scenarios, the use of limited ensemble members can cause aliasing of ENSO variability in ensemble means[4]. In a sense, our approach has treated the different reconstructions as different "models". It is thus a natural extension of our analysis to consider the possibility that some of the uncertainty regarding future tropical anthropogenic trends[39] (and their potential worldwide impact[6]) in coupled GCMs may similarly be due to different ENSO variations within the model ensembles. Our study provides a consistent historical Indo-Pacific SST trend with which to validate and verify climate models used for projections of future climate change.

Methods

a) Optimal Perturbation Filter

The climate system is often characterized by a notable separation between the dominant time scales of interacting processes. For example, compared to the much longer timescales of the ocean, weather varies so rapidly that it can be considered to have almost no

memory; its forcing of the ocean may be approximated by white noise. More generally, for some systems where nonlinear processes decorrelate much more rapidly than linear processes, anomaly evolution may be approximated in a coarse-grained sense as a linear dynamical system driven by white noise[40], or

$$\frac{d\mathbf{x}}{dt} = \mathbf{A}\mathbf{x} + \mathbf{B}\boldsymbol{\xi}, \tag{1}$$

where $\mathbf{A}$ is a deterministic feedback matrix, $\mathbf{x}$ is the climate anomaly state vector where x_i is the anomaly at location i, ξ_i is Gaussian white noise at location i, and $\mathbf{B}$ is a matrix allowing for spatial coherence in the temporally white forcing. When $\mathbf{B}$ is constant (1) is sometimes called "multivariate red noise"[26], in analogy with its univariate counterpart. The most probable forward solution of (1) at time $t + \tau$ is then

$$\hat{\mathbf{x}}(t+\tau) = \exp(\mathbf{A}\tau)\,\mathbf{x}(t) = \mathbf{G}(\tau)\mathbf{x}(t), \tag{2}$$

where $\mathbf{G}(\tau) = \exp(\mathbf{A}\tau)$. For multivariate red noise, a LIM can be constructed estimating $\mathbf{A}$ from data in an inverse sense as ${\tau_0}^{-1} \ln\{\mathbf{C}(\tau_0)\mathbf{C}(0)^{-1}\}$, where $\mathbf{C}(\tau_0)$ is the lag-covariance matrix $\langle\, \mathbf{x}(t+\tau_0)\mathbf{x}(t)^{\mathrm{T}}\rangle$ for some specified lag τ_0. To complete the LIM, the suitability of the linear approximation (1) must be tested (for example, $\mathbf{A}$ should not depend upon the choice of τ_0[25]).

LIMs of 3-month running mean tropical Indo-Pacific SST anomalies demonstrate that (1) represents both SST anomaly evolution statistics and the case-to-case evolution of individual events quite well[23,25-28]. Importantly, while $\mathbf{A}$ is stable (its eigenvalues all have negative real parts) it is also nonnormal[23] (its eigenvectors are nonorthogonal) because of asymmetries in the physical system[41], allowing transient anomaly growth to occur over limited periods due to modal interference before anomalies ultimately decay[23,25-28]. The maximum anomaly growth possible over a time interval $[0, \tau_e]$ is initiated by the "optimal" initial condition $\tilde{\mathbf{x}}(t) = \boldsymbol{\phi}_\mathbf{1}$, which evolves into

$$\tilde{\mathbf{x}}(t+\tau_e) = \mathbf{G}(\tau_e)\boldsymbol{\phi}_\mathbf{1} = \gamma_1\boldsymbol{\psi}_\mathbf{1}, \tag{3}$$

where the singular vector pair $\boldsymbol{\phi}_\mathbf{1}$ and $\boldsymbol{\psi}_\mathbf{1}$ are the normalized dominant right and left singular vectors of $\mathbf{G}(\tau_e)$ and γ_1 is the associated singular value[25]. The *potential* growth of the dominant right singular vector, greatest for $\tau_e = 6 - 9$ months, is realized by the *actual* evolution of observed ENSO events of both signs[23,25-28]. Thus, to use LIM to filter out the

evolving ENSO phenomenon we need to remove the optimal initial condition and its subsequent evolution.

We construct a filter specifically removing only variability that actually *evolves* from the optimal initial condition through a mature ENSO event. Since the right and left singular vectors each form orthogonal sets only at $\tau = 0$ and $\tau = \tau_e$, respectively, the filter must be applied iteratively. First, the projection on $\boldsymbol{\phi_1}$ at time $t = t_i$ is determined and its subsequent linear evolution over the time interval $t = [t_i, t_i + \tau_1]$ is removed. Then, t is incremented by 3 (since we use seasonal means), the projection on $\boldsymbol{\phi_1}$ of the residual anomaly at time $t = t_i + 3$ is determined, and the process is repeated. The procedure thus takes the form:

for $t = 0$: $\alpha(0) = \boldsymbol{\phi_1}(\tau_e) \cdot \mathbf{x}(0)$,
$\mathbf{R}(0) = \mathbf{x}(0) - \alpha(0)\mathbf{G}(0)\boldsymbol{\phi_1}(\tau_e)$
for $t = 3$: $\alpha(3) = \boldsymbol{\phi_1}(\tau_e) \cdot \big(\mathbf{x}(3) - \alpha(0)\mathbf{G}(3)\boldsymbol{\phi_1}(\tau_e)\big)$,
$\mathbf{R}(3) = \mathbf{x}(3) - \alpha(0)\mathbf{G}(3)\boldsymbol{\phi_1}(\tau_e) - \alpha(3)\mathbf{G}(0)\boldsymbol{\phi_1}(\tau_e)$
…
for $t = n$: $\alpha(n) = \boldsymbol{\phi_1}(\tau_e) \cdot \big(\mathbf{x}(n) - \sum_3^{\tau_1} \alpha(n-\tau)\mathbf{G}(\tau)\boldsymbol{\phi_1}(\tau_e)\big)$,
$\mathbf{R}(n) = \mathbf{x}(n) - \sum_0^{\tau_1} \alpha(n-\tau)\mathbf{G}(\tau)\boldsymbol{\phi_1}(\tau_e)$

where α is the projection of $\boldsymbol{\phi_1}(\tau_e)$ on the anomaly at that point in the iteration and the summations are over τ. Therefore, for $t \geq \tau_1$ the residual determined by removing variability that linearly evolved from $\boldsymbol{\phi_1}(\tau_e)$ is

$$\mathbf{R}(t) = \mathbf{x}(t) - \sum_0^{\tau_1} \alpha(t-\tau)\mathbf{G}(\tau)\boldsymbol{\phi_1}(\tau_e) \qquad (4)$$

We remove the evolution of a projection on $\boldsymbol{\phi_1}(\tau_e = 3)$ over τ_1=21 months in our filter. While τ_e= 3 yields an evolving structure that is most representative of ENSO, the evolution of $\boldsymbol{\phi_1}(\tau_e = 6)$ is quite similar and filtering it yields similar results (see SOM for a detailed discussion of the filter design and tests for robustness). Spin-up of the iteration is small, with results independent of the starting date (e.g., starting in 1910 rather than 1891) apart from the first few years. Note that we assume the dynamical evolution of $\boldsymbol{\phi_1}$ does not significantly change over the entire data record; this assumption is shown to be valid in the supplemental online.

For ENSO, it turns out that the evolution of $\boldsymbol{\phi_1}$ into $\boldsymbol{\psi_1}$ can be largely represented by a relatively small eigenmode subspace of $\mathbf{A}$[20,23,25,28], which initially suggested an approach to filter dynamical ENSO evolution in which all projection of the data on this subspace is

removed[20,23]. The resulting "eigenmode filter" efficiently removes the evolving ENSO structure, but also removes variability not part of the evolution of $\boldsymbol{\phi_1}$ into $\boldsymbol{\psi_1}$ that nevertheless projects onto the eigenmode subspace – potentially including a portion of the trend[20] (see Supplementary material). Additionally, the eigenmode filter is much less robust than the optimal perturbation filter, which seems due to the fact that individual eigenmodes are much more sensitive to small differences in the background state than are the leading singular vectors[42,43] Obviously, the most complete representation of the right singular vector is obtained by using all the eigenmodes, which would make the filter trivial, so some stopping criteria must be applied to limit the number of eigenmodes in the approximation. In practice, there is no unique method to determine the stopping criteria so there is no unique definition of this subspace, potentially allowing different combinations of eigenmodes to be used to approximate the same singular vector[20,23,25] This problem becomes more severe when approximating the corresponding singular vectors across different datasets. Consequently, because of the strong nonnormality of the eigenmodes, the subspace that is removed by the eigenmode filter can vary substantially from dataset to dataset (see Supp. Fig. 27). Thus, applying the eigenmode filter to the different datasets yields greater differences amongst the ENSO-residual trend and variability than does the optimal perturbation filter.

b) Data used

The data used in this study are 3-month seasonal mean three dimensional ocean temperature and surface wind stress fields from the Simple Ocean Data Assimilation version 2.1.6 (SODA[44]) for the period 1958-2007, and 1891-2010 seasonal mean SSTs from 4 centennial reconstructions: Hadley Centre Sea Ice and SST dataset version 1.1[45] (hereafter HadISST), the National Oceanic and Atmospheric Administration Extended Reconstruction SST version 3b dataset[46] (hereafter ERSST), Lamont Doherty Earth Observatory SST version 2[47](hereafter KAPLAN), Centennial in Situ Observation Based Estimates of SST[48] (hereafter COBE). The fields are interpolated to a 2°x2° latitude/longitude grid and the SODA temperature data is interpolated in the vertical to levels at 15m intervals from 5m to 290m. Data are prefiltered by retaining the first 20 empirical orthogonal functions (EOFs), calculated using SSTs for the reconstructions and 5m temperatures for SODA (wind stress and three-dimensional temperature fields are calculated by regression to the 5m EOFs),

which explains 78% of the total SODA variance. This study also uses 1870-2008 monthly mean sea level pressure anomalies from Hadley Centre SLP version 2[49] which are available on a 5°x5° latitude/longitude grid. Linear trends are calculated in this study using the method of least-squares. Analysis of the SST reconstruction datasets uses the common period 1891-2010, but trends are displayed for 1900-2010 to match 20th century analyses.

Acknowledgements. The authors thank Joe Barsugli, Cecile Penland, Mike Alexander, Gil Compo, Prashant Sardeshmukh, Randy Dole, Bill Neff, Robin Webb, and Clara Deser for insightful comments. This work was supported by grants from the NOAA OAR CVP Program and NSF AGS #1125561 and 1035325.

References

1. Diaz, H. F. & Markgraf V. El Niño: Historical and paleoclimatic Aaspects of the Southern Oscillation. Cambridge University Press, Cambridge, 476 pp. (1992)

2. Glantz, M. H. Currents of Change: Impacts of El Nino and La Nina on climate and society. Cambridge University Press, Cambridge, 252 pp. (2001)

3. Alexander, M. A., Blade, I., Newman, M., Lanzante, J. R., Lau, N.-C. & Scott, J. D. The Atmospheric Bridge: The influence of ENSO teleconnections on air-sea interaction over the global oceans. *J. Climate* **15**, 2205-2231 (2002)

4. Solomon, A. and the US CLIVAR Decadal Predictability Working Group. Distinguishing the roles of natural and anthropogenically forced decadal climate variability: Implications for prediction. *Bull. Amer. Met. Soc.* **92**, 141-156, http://dx.doi.org/10.1175/2010BAMS2962.1 (2011

5. Deser, C., Phillips, A. S. & Alexander, M. A. Twentieth century tropical sea surface temperature trends revisited. *Geophys. Res. Lett*. **37**, L10701, http://dx.doi.org/10.1029/2010GL043321 (2010)

6. Shin, S.-I. & Sardeshmukh, P. D. Critical influence of the pattern of Tropical Ocean warming on remote climate trends. *Clim. Dyn.* **36**, 1577-1591 (2011)

7. Collins, M. et al. The impact of global warming on the tropical Pacific Ocean and El Niño. *Nature Geoscience* **3**, 391-396, DOI:10.1038/NGEO868 (2010)

8. Clement, A. C., Seager, R., Cane, M. A. & Zebiak, S. E. An ocean dynamical thermostat. *J. Climate* **9**, 2190–2196 (1996)

9. Sun, D.-Z. & Liu, Z. Dynamic ocean-atmosphere coupling: a thermostat for the tropics.

Science 272, 1148–1150 (1996)

10. Seager, R. & Murtugudde, R. Ocean dynamics, thermocline adjustment, and regulation of tropical SST. *J. Climate* **10**, 521–534 (1997)

11. Cane, M. A., Clement, A. C., Kaplan, A., Kushnir, Y., Pozdnyakov, D., Seager, R., Zebiak, S. E. & Murtugudde, R. Twentieth century sea surface temperature trends. *Science* **275**, 957–960 (1997)

12. Knutson, T. R. & Manabe, S. Time-mean response over the tropical Pacific to increased CO2 in a coupled ocean–atmosphere model. *J. Climate* **8**, 2181–2199 (1995)

13. Meehl, G. A. & Washington, W. El Niño-like climate change in a model with increased atmospheric CO2 concentrations. *Nature* **382**, 56–60 (1996)

14. Xie, S.-P., Deser, C., Vecchi, G. A., Ma, J., Teng, H. & Wittenberg, A. T. Global warming pattern formation: sea surface temperature and rainfall. *J. Climate* **23**, 966–986 (2010)

15. Held, I. M. & Soden, B. J. Robust responses of the hydrological cycle to global warming. *J. Climate* 19, DOI:10.1175/JCLI3990.1 (2006)

16. Vecchi, G. A. & Soden, B. J. Global warming and the weakening of the tropical circulation. *J Climate* **20**, 4316–4340 (2007)

17. Schneider, E. K., Lindzen, R. S. & Kirtman, B. P. A tropical influence on global climate. *J. Atmos. Sci.* **54,** 1349-1358 (1997)

18. Shin S.-I. & Sardeshmukh, P. D. Critical influence of the pattern of Tropical Ocean warming on remote climate trends. *Clim. Dyn***. 36,** 1577-1591 (2010)

19. Newman, M., Sardeshmukh, P. D. & Penland, C. How important is air-sea coupling in ENSO and MJO evolution? *J. Climate* **22**, 2958–2977 (2009)

20. Compo, G.P. & Sardeshmukh, P. D. Removing ENSO-related variations from the climate record. *J. Climate* **23**, 1957-1978. http://dx.oi.org/10.1175/2009JCLI2735.1 (2010)

21. Thompson, D. W. J., Wallace, J. M., Jones, P. D. & Kennedy, J. J. Identifying signatures of natural climate variability in time series of global-mean surface temperature: methodology and insights. *J. Climate* **22**, 6120–6141 (2009)

22. Tung, K. K. & Zhou, J. The Pacific's response to surface heating in 130 yr of SST: La-Niña-like or El Niño-like? *J. Atmos. Sci.* **67**, 2649-2657 (2010)

23. Penland, C. & Matrosova, L. Studies of El Nino and interdecadal variability in tropical sea surface temperatures using a nonnormal filter. *J. Climate* **19**, 5796-5815 (2006)

24. McPhaden, M. J. Genesis and evolution of the 1997–1998 El Niño. *Science* **283**, 950–954, http://dx.doi.org/10.1126/science.283.5404.950 (1999)

25. Penland, C. & Sardeshmukh, P. D. The optimal growth of tropical sea surface temperature anomalies. *J. Climate* **8**, 1999–2024 (1995)

26. Newman, M., Shin, S.-I. & Alexander, M. A. Natural variation in ENSO flavors. *Geophys. Res. Lett.* L14705, http://dx.doi.org/10.1029/2011GL047658 (2011)

27. Penland, C. & Magorian, T. Prediction of Niño 3 sea surface temperatures using linear inverse modeling. *J. Climate* **6**, 1067–1076 (1993)

28. Newman, M., Alexander, M. A. & Scott, J. D. An empirical model of tropical ocean dynamics. *Climate Dynamics* **37**, 1823-1841, http://dx.doi.org/10.1007/s00382-011-1034-0 (2011)

29. Penland, C. & Matrosova, L. A balance condition for stochastic numerical models with application to the El Niño-Southern Oscillation. *J. Climate* **7**, 1352-1372 (1994)

30. Bjerknes, J. Atmospheric teleconnections from the equatorial Pacific. *Monthly Weather Review* **97**, 163– 172 (1969)

31. Karnauskas, K. B., Seager, R., Kaplan, A., Kushnir, Y. & Cane, M. A. Observed strengthening of the zonal sea surface temperature gradient across the equatorial Pacific Ocean. *J. Climate* **22**, 4316–4321, http://dx.doi.org/10.1175/2009JCLI2936.1 (2009)

32. Vecchi, G. A., Soden, B. J., Wittenberg, A. T., Held, I. M., Leetmaa, A. & Harrison, M. J. Weakening of tropical Pacific atmospheric circulation due to anthropogenic forcing. *Nature* **441**, 73-76, doi:10.1038/nature04744 (2006)

33. Bunge, L. & Clarke, A. J. A verified estimation of the El Nino index NINO3.4 since 1877. *J. Climate* **22**, 3979-3992 (2009)

34. Compo, G. et al. The Twentieth Century Reanalysis Project. *Quarterly J. Roy. Meteorol. Soc*. **137**, 1-28, DOI: 10.1002/qj.776 (2011)

35. Guan, B. & Nigam, S. Pacific sea surface temperatures in the twentieth century: An evolution-centric analysis of variability and trend. *J. Climate* **21**, 2790-2809 (2008)

36. Lau, K.-M. & Weng, H. Interannual, decadal–interdecadal, and global warming signals in sea surface temperature during 1955–97. *J. Climate* **12**, 1257-1267 (1999)

37. Hoerling, M. & Kumar, A. A perfect ocean for drought. *Science* **299,** 691-694 (2003)

38. Solomon, A. & Newman, M. Decadal predictability of tropical Indo-Pacific Ocean

temperature trends due to anthropogenic forcing. *Geophys. Res. Lett.* **38**, L02703, http://dx.doi.org/10.1029/2010GL045978 (2011)

39. Collins, M. & the CMIP Modelling Groups. El Niño- or La Niña-like climate change? *Climate Dyn*, **24**, 89–104. (2005)

40. Hasselmann, K. Stochastic climate models. Part I. Theory. *Tellus* **28**, 474-485 (1976)

41. Moore, A. M. & Kleeman, R. The nonnormal nature of El Niño and intraseasonal variability. *J. Climate* **12**, 2965–2982 (1999)

42. Borges, M. & Sardeskmukh, P. D. Application of perturbation theory to the stability analysis of realistic atmospheric flows. *Tellus* **49**, 321-336 (1997)

43. Penland, C. & Sardeshmukh, P. D. Error and sensitivity analysis of geophysical systems. *J. Climate* **8**, 1988-1998 (1995)

44. Carton, J. A. & Giese, B. S. A reanalysis of ocean climate using Simple Ocean Data Assimilation (SODA). *Mon. Wea. Rev.* **136**, 2999-3017 (2008)

45. Rayner, N. A. et al. Global analyses of sea surface temperature, sea ice, and night marine air temperature since the late nineteenth century. *J. Geophys. Res*. **108**, http://dx.doi.org/10.1029/2002JD002670 (2003)

46. Smith, T. M., Reynolds, R. W., Peterson, T. C. & Lawrimore, J. Improvements to NOAA's historical merged land-ocean surface temperature analysis (1880-2006). *J. Climate* **21**, 2283-2296 (2008)

47. Kaplan, A. et al. Analyses of global sea surface temperature 1856–1991. *J. Geophys. Res*. **103**, 18,567–18,589, http://dx.doi.org/10.1029/97JC01736 (1998)

48. Ishii, M., Shouji, A., Sugimoto, S. & Matsumoto, T. Objective analyses of SST and marine meteorological variables for the 20th century using ICOADS and the Kobe Collection. *Int. J. Climatol.* **25**, 865–879 (2005)

49. Allan, R. J. & Ansell T. J. A new globally complete monthly historical mean sea level pressure data set (HadSLP2): 1850–2004. *J. Climate* **19**, 5816–5842, doi:10.1175/JCLI3937.1 (2006)

Figure Captions:

Figure 1: Unfiltered SST trends, in units of °C/100 years**,** 1900-2010. (A) HadISST. (B) ERSST. (C) COBE. (D) KAPLAN (see Methods Section b for dataset descriptions). Stippling indicates trends are significant beyond the 95% confidence level based on time series calculated from linear inverse models constructed with lag covariance and noise statistics from each dataset (see Methods Section a for a discussion of this technique).

Figure 2: First empirical orthogonal function of 1958-2007 SODA seasonal mean SST anomalies, regressed to ocean temperature and wind stress anomalies (explains 34.7% percent of the total seasonal mean SST variance). Contour interval equal to 0.02. A) At 5 meters. B) Along the equator. Thick blue contour marks the climate mean 20°C isotherm depth. C) At 160°W. D) Normalized time series of first principal component. Unfiltered mean tropical Indo-Pacific SST anomalies shown with red line. Time series normalized by 18.8°C (leading principal component) and 0.26°C (SSTs).

Figure 3: SODA ENSO-residual ocean temperature and wind stress trend pattern and time series. A 1-year running mean has been applied to the data. Contour interval equal to 0.5°C/100 years and wind stress in units of N/m^2/100 years in (A), (B), (C). A) At 5 meters. Blue rectangles mark the warm pool (18°N-18°S, 60°-165°E) and cold tongue (4°N-4°S, 170°E-70°W) regions. B) Along the equator. Thick blue contour marks the climate mean 20°C isotherm depth. C) At 160°W. D) Cold tongue and warm pool time series for unfiltered (black) and ENSO-residual (red) data, in units of °C.

Figure 4: HadISST(red), ERSST(blue), KAPLAN(magenta), and COBE(black) time series, in units of °C. A one-year running mean has been applied to the data. (A) Unfiltered cold tongue region. (B) ENSO-residual cold tongue region. (C) Unfiltered warm pool region. (D) ENSO-residual warm pool region.

Figure 5: ENSO-residual SST trends, in units of °C/100 years, 1900-2010. (A) HadISST. (B) ERSST. (C) COBE. (D) KAPLAN. Stippling indicates trends are significant beyond the

95% confidence level based on ENSO-residual time series from LIMs constructed with lag covariance and noise statistics from each dataset.

Figure 6: HadSLP2 anomalies for the 1870-2010 period (relative to a 1891-2010 climatology) smoothed with a 10-year running mean, in units of hPa. Unfiltered time series shown in black. ENSO-residual time series from data where the filter is constructed with SLP alone(SST alone) shown in red(blue dash). Regions as defined in ref. 5. (A) Indian Ocean/West Pacific averages. (B) Central-east Pacific averages. (C) Indian Ocean/West Pacific minus Central-east Pacific averages.

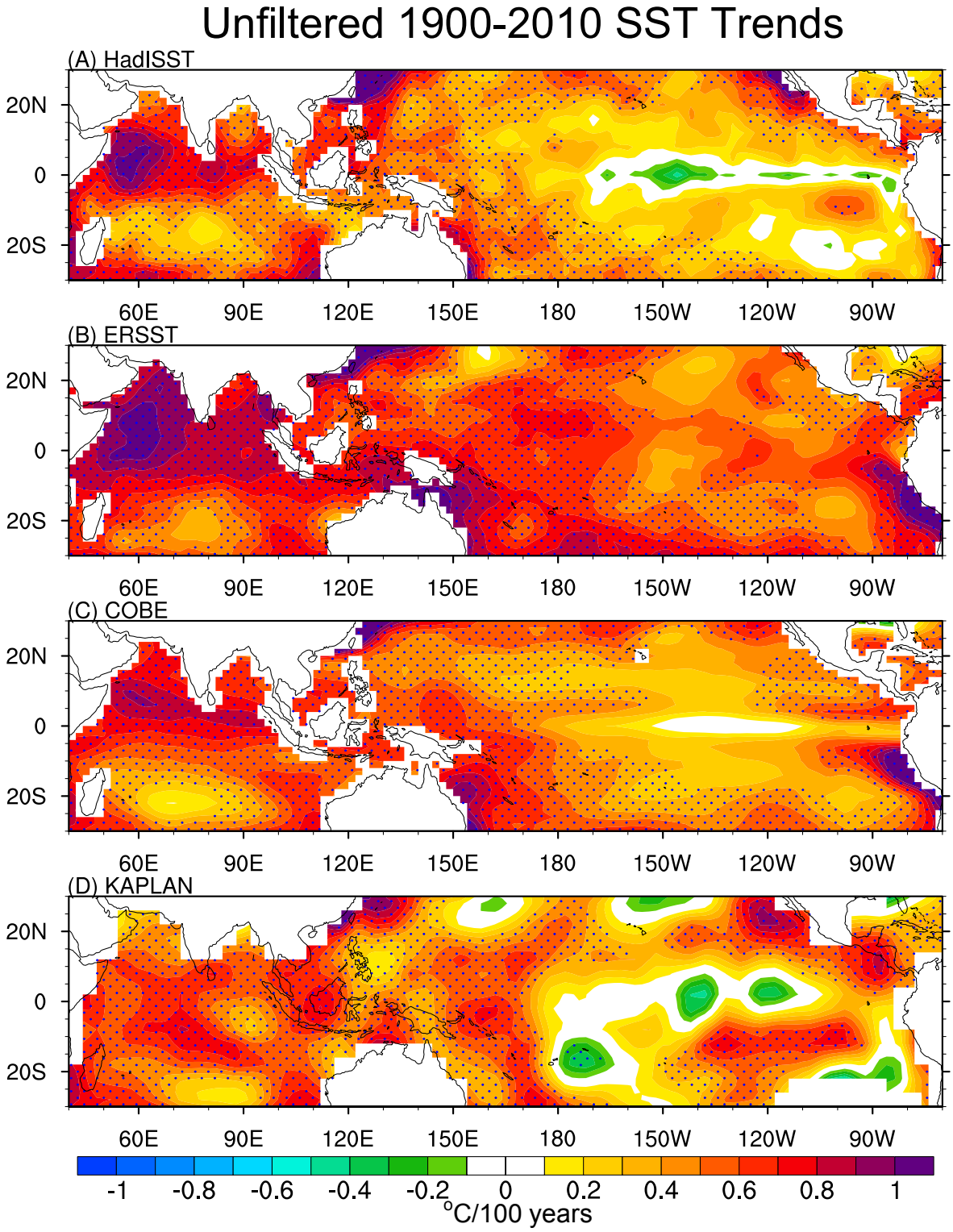
Unfiltered 1900-2010 SST Trends
(A) HadISST
(B) ERSST
(C) COBE
(D) KAPLAN
20N
0
20S
60E
90E
120E
150E
180
150W
120W
90W
-1
-0.8
-0.6
-0.4
-0.2
0
0.2
0.4
0.6
0.8
1
°C/100 years

SODA 1958-2007 Temperature Anomalies

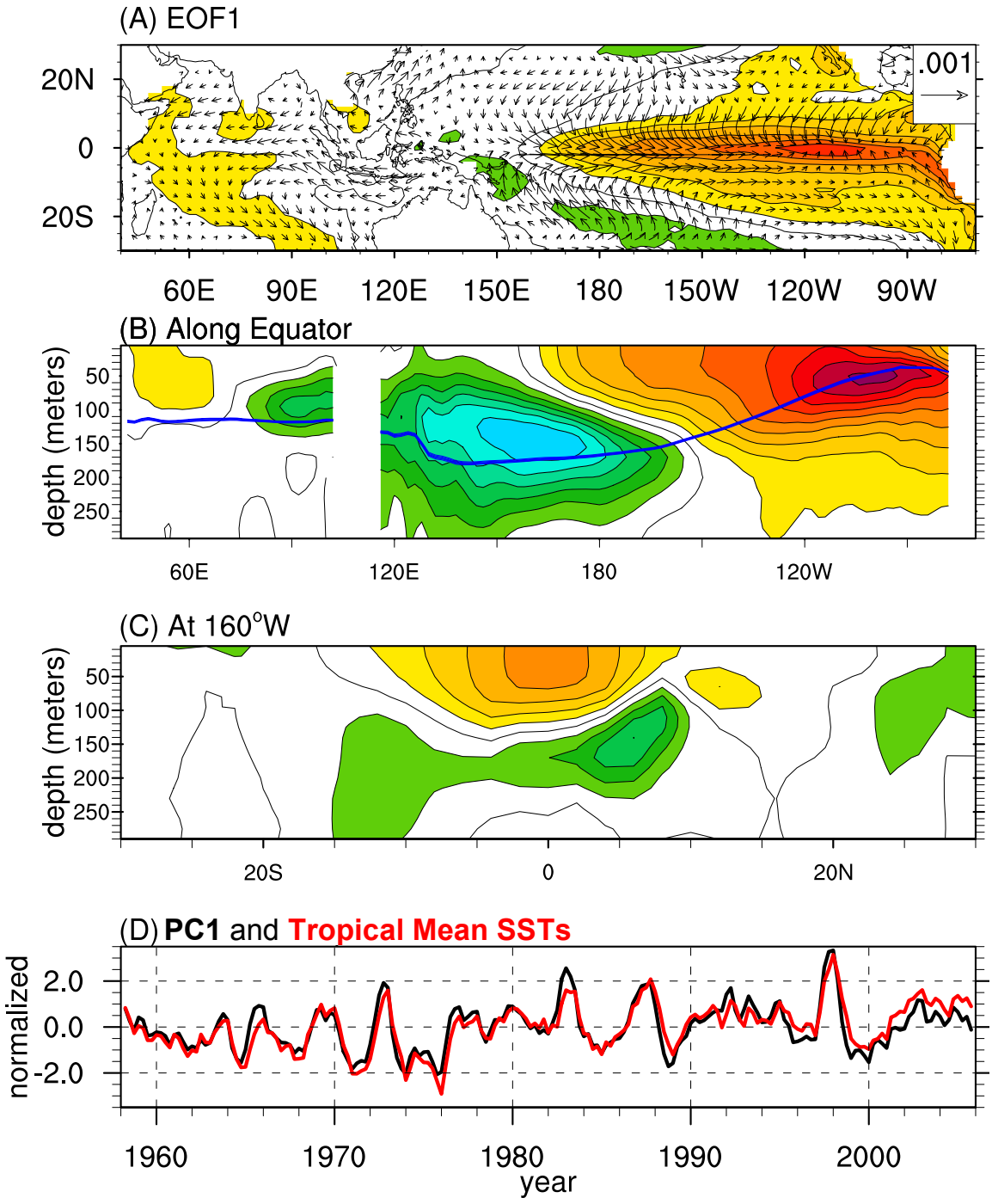

SODA 1958-2007 ENSO-Residual Trends

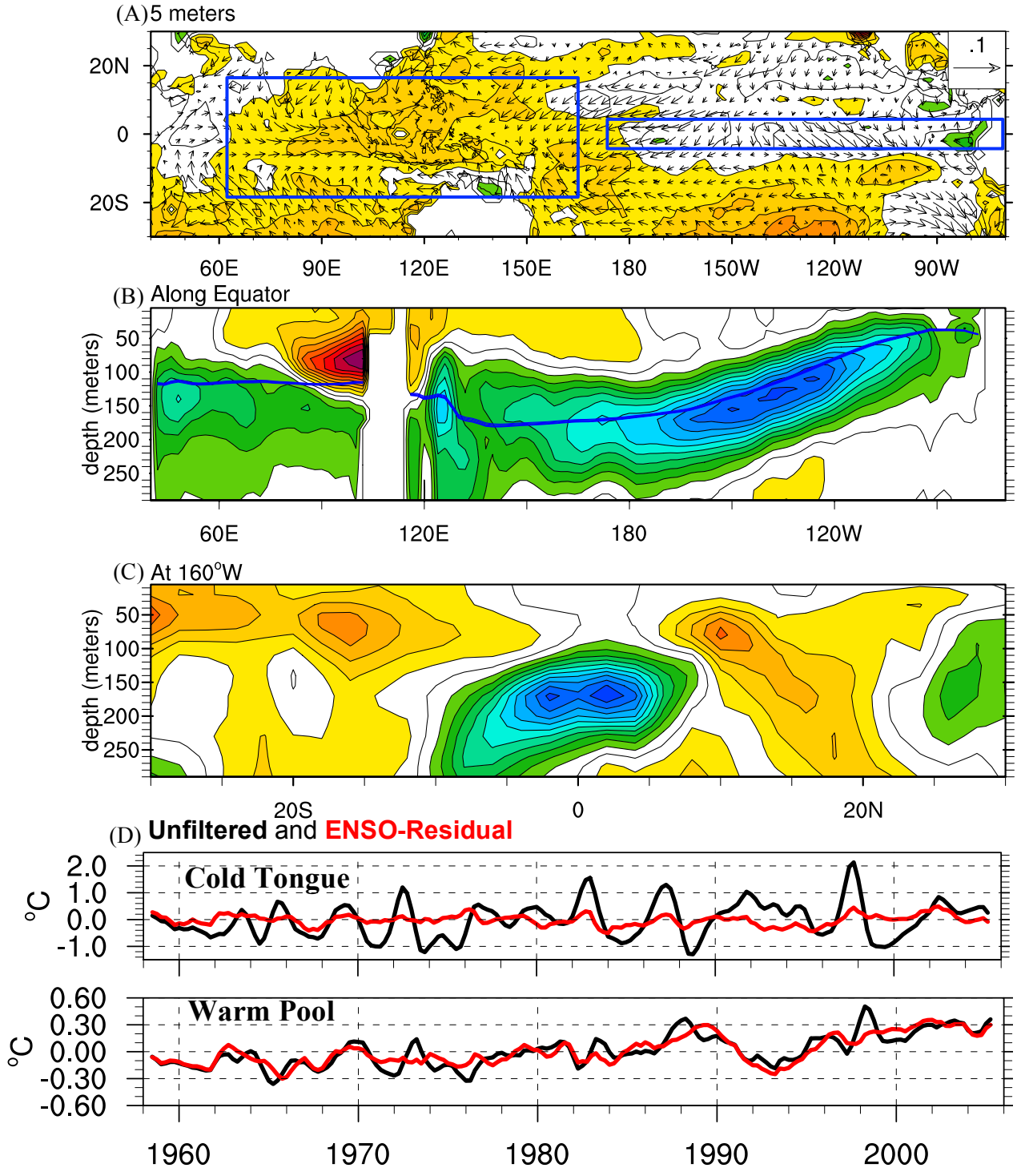

Cold Tongue and Warm Pool Time Series

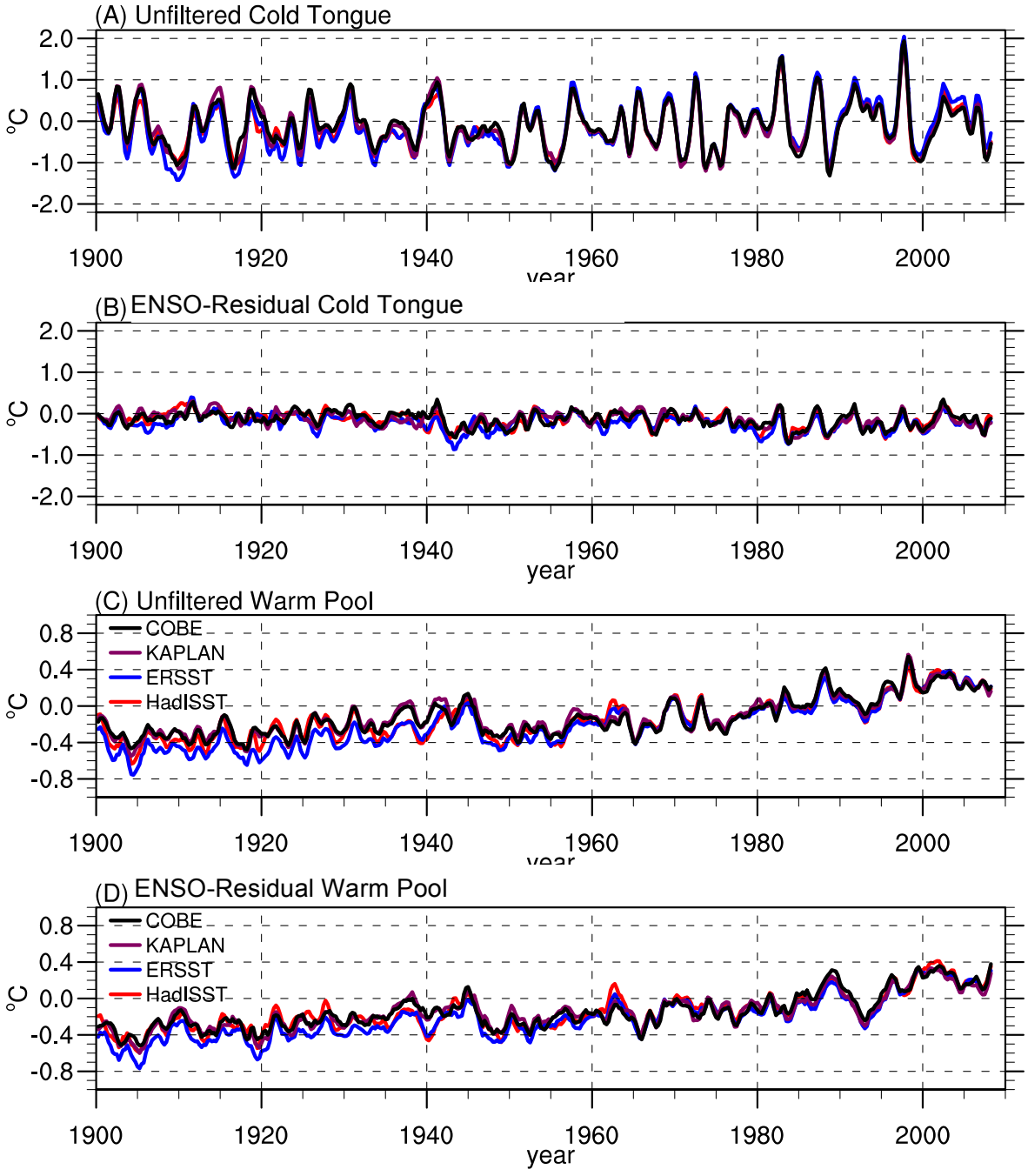

1900-2010 ENSO-Residual SST Trends

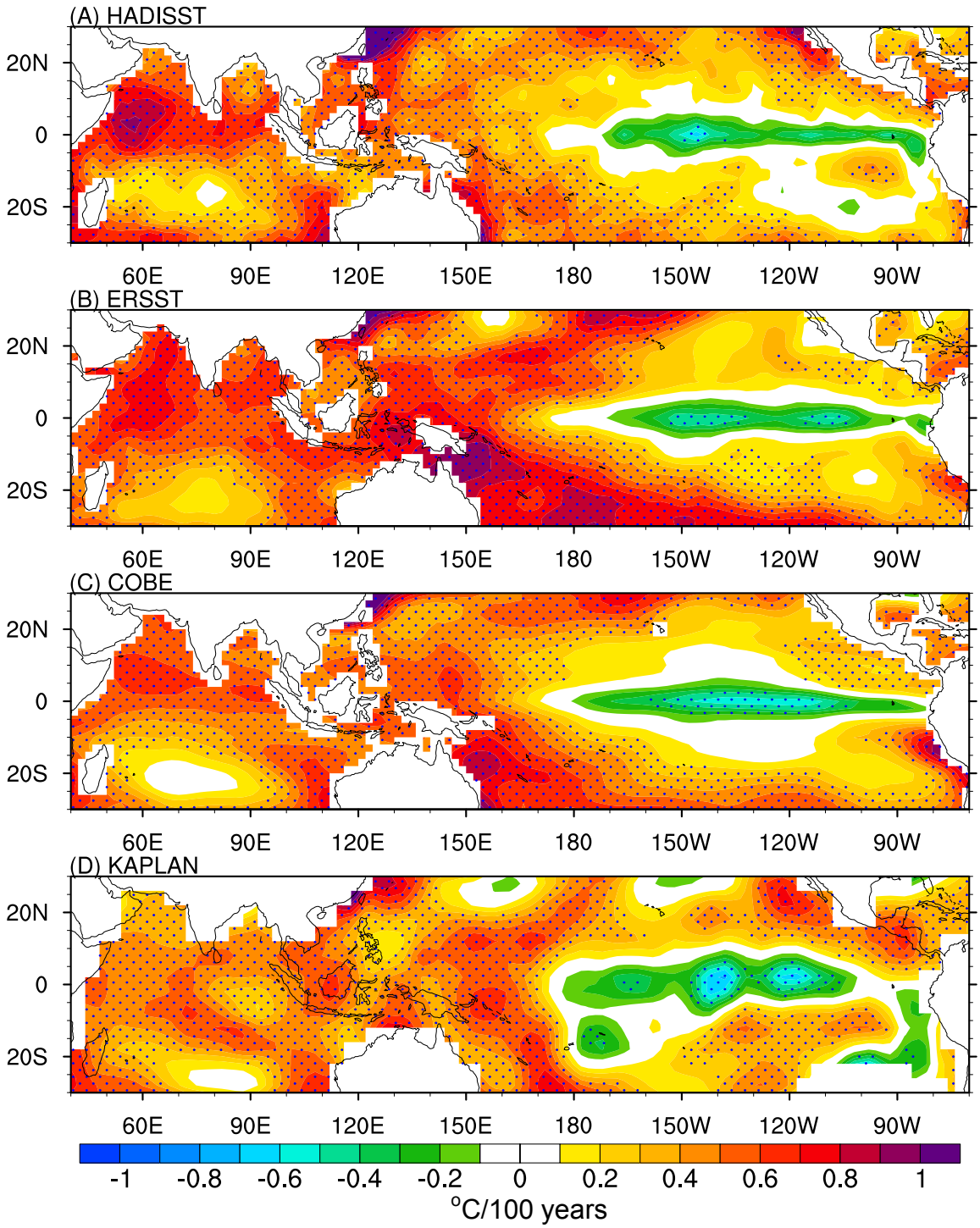

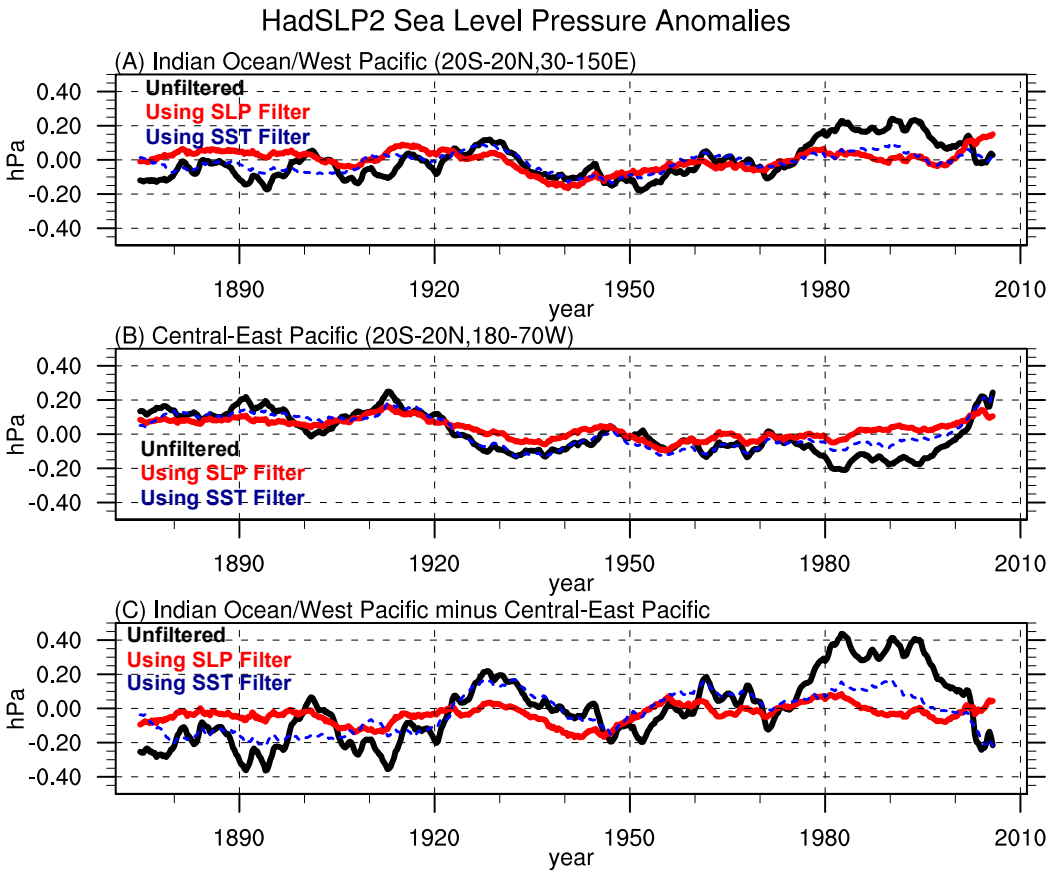
HadSLP2 Sea Level Pressure Anomalies
(A) Indian Ocean/West Pacific (20S-20N,30-150E)
Unfiltered
Using SLP Filter
Using SST Filter
hPa
0.40
0.20
0.00
-0.20
-0.40
1890
1920
1950
1980
2010
year
(B) Central-East Pacific (20S-20N,180-70W)
Unfiltered
Using SLP Filter
Using SST Filter
hPa
0.40
0.20
0.00
-0.20
-0.40
1890
1920
1950
1980
2010
year
(C) Indian Ocean/West Pacific minus Central-East Pacific
Unfiltered
Using SLP Filter
Using SST Filter
hPa
0.40
0.20
0.00
-0.20
-0.40
1890
1920
1950
1980
2010
year